Prediction of turning performances using an equivalent oblique cutting model

LEFI ABDELLAOUI (lefiabdellaoui@yahoo.fr)
Institut Préparatoire aux études d'ingénieurs de Bizerte
Hassen KHLIFI
https://orcid.org/0000-0001-8926-7796
Wassila BOUZID SAI

Research Article

Keywords: Turning performances, Tool/chip interface temperature, Heat equation, Finite Difference Method (FDM), Laplace transform, Partition coefficient

Posted Date: February 10th, 2022

DOI: https://doi.org/10.21203/rs.3.rs-1331545/v1

Prediction of turning performances using an equivalent oblique cutting model

Lefi ABDELLAOUI [1,2], Hassen KHLIFI [1], Wassila BOUZID SAI [1]

[1] Unité de Génie de Production Mécanique et Matériaux UGPMM, ENIS, Sfax, Tunisie.

[2] Université de Carthage (University of Carthage), IPEST, 2078 La Marsa, Tunisie

Corresponding author: *Lefi ABDELLAOUI (lefiabdellaoui@yahoo.fr)*

Abstract

The main purpose of this paper is to predict the performances of the turning process using an equivalent oblique cutting model. Based on the real tool, an equivalent cut geometry is performed considering the effects of nose and edge radii. Edge direction and normal cutting angles, uncut chip thickness and depth of cut were redefined by their equivalent values and then used as new inputs. Turning performances, such as cutting force components, cutting temperatures and tribology parameters at the tool/chip interface, were predicted over a wide range of cutting conditions. The position of the maximum temperature at the tool/chip interface and its value are determined by solving the heat equation in the chip using the Finite Difference Method (FDM). Different assumptions were concluded, and the thermal problem is simply resolved using Laplace transform. Acceptable agreement was concluded between experimental cutting force components and those predicted from the equivalent oblique cutting model. It can thus be concluded that the equivalent model of cut is highly recommended to predict turning performances and to study crater wear and tool life.

Keywords

Turning performances, Tool/chip interface temperature, Heat equation, Finite Difference Method (FDM), Laplace transform, Partition coefficient.

Introduction

Turning represents an essential process in manufacturing components in which tool geometry performs material removal. It can be used for a variety of work materials to generate different shapes with a better workpiece quality such as roughness, geometric and dimensional specifications and surface finish aspects.

Machined materials are subject to plastic deformations. More than 90% of mechanical work applied to workpiece material transforms to thermal energy which is spread in tool, workpiece, and chip [1]. The percentage of cutting heat flowing into the cutting tool varying from 2% and 18%, into the workpiece from 1% to 20% and into the chip from 74% to 96% [2]. According to Puls et al. [3], elevated tool/chip interface temperature accelerates tool wear and causes a thermal expansion of cutting tool which causes cutting edge displacement and worsens machined surface quality. On the other hand, it is well known that the direct measurement of tool/chip interface temperature in machining is very difficult. Huang et al. [4] have developed an on-line inverse technique to estimate the temperature field at the tool/chip interface of a turning tool using temperatures measured at some sensor-accessible locations. According to Abdil Kus et al. [5], it is necessary to use different measuring techniques to obtain consistent temperature data. They have estimated tool temperature by simultaneous measurement employing both a K-type thermocouple and an infrared radiation pyrometer.

Predicting performances, such as cutting forces, tool/chip interface temperature, heat partition between workpiece, tool and chip, tribology parameters and tool wear, are highly recommended by the machining community. The models commonly used by researchers are analytical, numerical, and mechanistic. The analytical approach allows to understand the physical phenomenon which occurs when metal cutting and predicts thermomechanical parameters over a wide range of cutting conditions. On the other hand, the numerical solutions provide a viable alternative to understand the machining process; however, its limitation consists in its ability to assimilate the complexity of machining problem.

Merchant was the pioneer who introduced the concept of shear angle [6]. Then, Lee and Shaffer have proposed an analytical model based on the slip line theory [7]. Later, Oxley introduced the first model based on the thermo-mechanical approach for the orthogonal cutting [8]. However, it was limited to a few industrial applications such as grooving and pipe cutting. For this reason, the oblique cutting modelling was highly recommended to study metal cutting with a complex geometry for each couple workpiece-tool (CWT).

The most recent thermomechanical approaches for oblique cutting were developed by Moufki et al. [9], Li et al. [10] and Abdellaoui and Bouzid. [11]. However, the effects of edge and nose radii are not explicitly considered. In fact, Nose radius has a significant effect on the geometry of uncut chip area, uncut chip thickness, cutting forces, chip geometry, heat generation, tool wear and surface finish during the turning process [12, 13]. On the other hand, cutting edge radius has a critical role in machining performances for small uncut chip thickness. Besides, when turning with a

larger tool nose radius, a large part of the uncut chip area will have a chip thickness less than the minimum uncut chip thickness. Thus, increasing nose radius increases the ploughing effect [14]. Recently, Khlifi et al. have developed a thermo-mechanical approach which leads to determine the equivalent geometry of the tool when considering tool nose and edge radii. The main idea consists in considering that the equivalent geometry induces the same cutting force as the real tool. Thus, equivalent cutting angle, equivalent direction angle, equivalent uncut chip thickness and equivalent depth of cut are defined for the new tool geometry.

In summary, accurate turning performances prediction still remains a challenge due to the complexity of contact phenomena at the tool/chip interface and tool geometry. For these reasons, establishing a predictive strategy with a good accuracy represents goal desired by researchers. That's why in the present research work, equivalent tool geometry was used, and a predictive model was developed. It permits to predict all thermomechanical parameters such as cutting force components, maximum tool/chip interface temperature and its position at the rake face and tool/chip contact parameters (contact length, temperature evolution, pressure, friction coefficient).

This paper is organized as follows: in section "Equivalent cutting for turning process", the equivalent model is presented, and its parameters are defined. In section "Thermomechanical modeling of equivalent cutting", two algorithms are presented. Algorithm 1 permits to determine equivalent geometry of the tool ($\kappa_r^{eq}$and α_n^{eq}) and the equivalent cutting parameters ($a_p^{eq}$and t_1^{eq}) and the second one predicts all equivalent thermomechanical parameters. Besides, in section "Study of the thermal problem in the chip" is presented and three approaches are used. Oxley's models, applied to equivalent oblique cutting, predicts the average tool/chip interface temperature. Then, a Finite Difference Method (FDM) is presented to solve the heat equation in the chip. Based on the numerical results, the thermal problem was simplified and solved using Laplace Transform. The analytical solution permits to predict the maximum tool/chip interface temperature and its position in the rake face. Finally, in the section "Experimental results and discussion", experimental tests are presented, and good agreement was noted between experimental force components and those predicted by equivalent model.

Equivalent cutting for turning process.

The real tool's geometry is characterized by many parameters such as nose radius r_ε, edge radius r_β, normal cutting angle α_n and the edge direction angle κ_r. Moreover, the turning operation is defined by cutting parameters which are depth of cut a_p, feed rate f and cutting speed V_c. Considering all these parameters makes the study more and more complex. Thus, working with the

equivalent tool geometry permits to avoid this complexity, mainly that of the nose and edge radii. The equivalent geometry is defined while conserving the same uncut chip area and values of the cutting force components compared to real cutting geometry [15].

In the present research work, equivalent parameters are defined using the work of Khlifi et al. [15]. Both effects of nose and edge radii are considered. Thus, the main equivalent cutting model is defined by four parameters which are the equivalent edge direction angle κ_r^{eq}, the equivalent depth of cut a_p^{eq}, the equivalent uncut chip thickness t_1^{eq} and the equivalent normal rake angle α_n^{eq} (Figures 1 and 2).

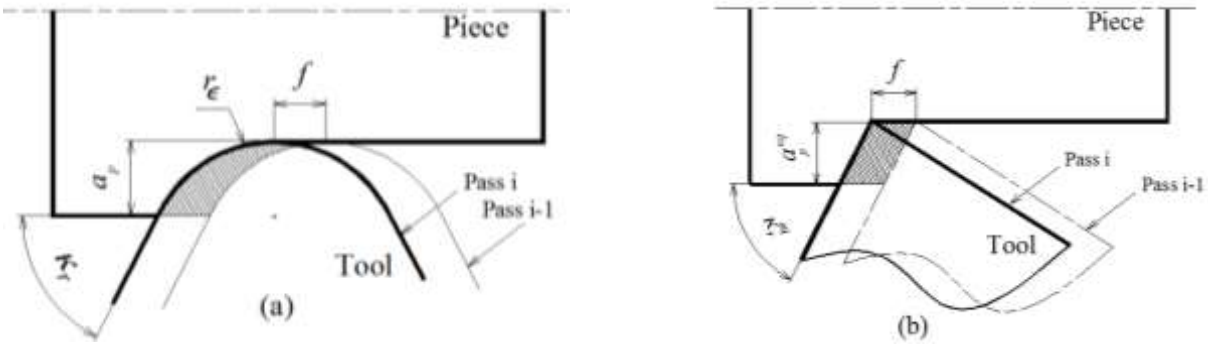

Figure 1. *View in the reference plan (P_r) of the turning process in finishing case $\left(a_p \leq r_\varepsilon(1-\cos\kappa_r)\right)$: (a) Real geometry, (b) equivalent geometry*

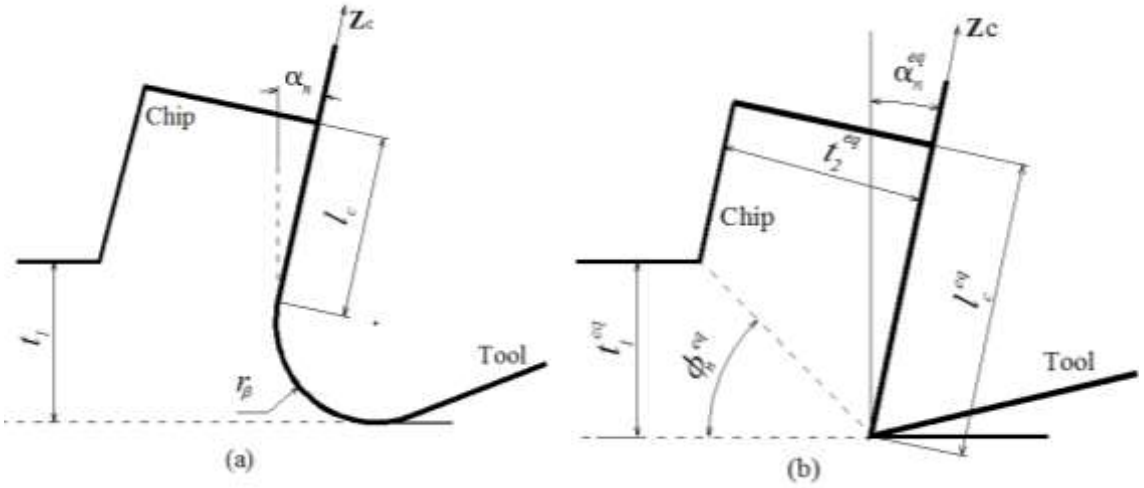

Figure 2. *View in the normal plan (P_n) of the turning process: Real geometry, (b) equivalent geometry*

Thermo-mechanical modeling of equivalent cutting

Thermomechanical parameters are defined and determined using the work of Abdellaoui and Bouzid [11, 13] and the work of Khlifi et al. (2019) [15]. Two algorithms are used to determine cutting forces, cutting temperatures and chip geometry (Figure 3). The first one allows to determine the equivalent geometry of the tool (κ_r^{eq} and α_n^{eq}) and the equivalent cutting parameters (a_p^{eq} and t_1^{eq}).

The second algorithm leads to determine the average tool/chip interface temperature and all other thermomechanical parameters for the equivalent cutting.

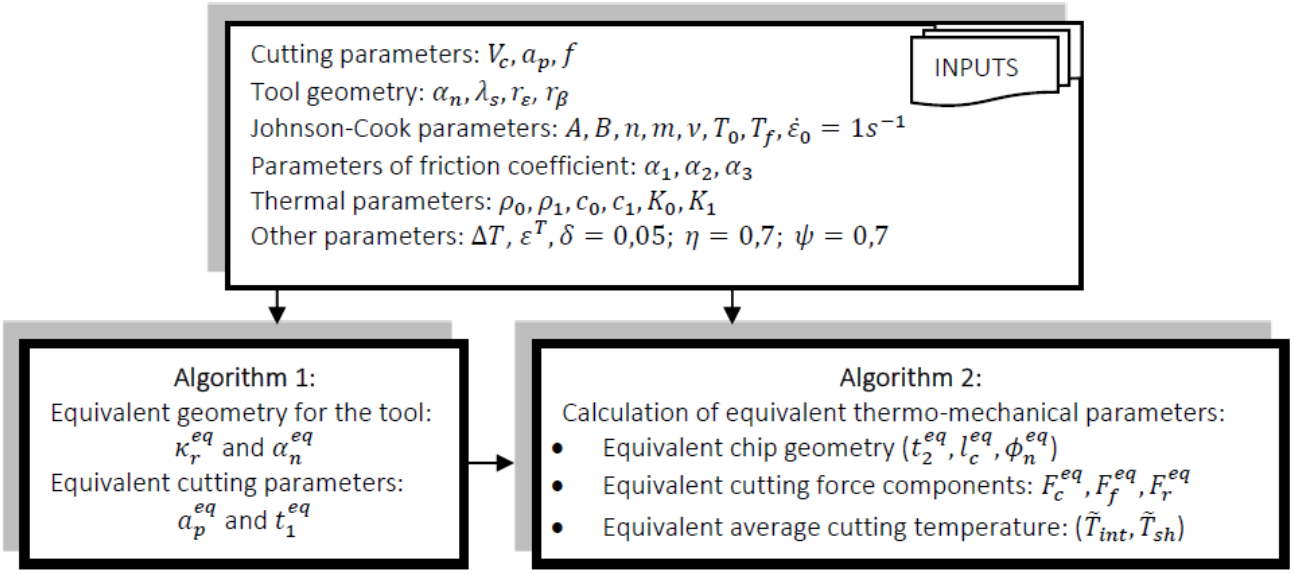

Figure 3. *Analytical algorithm for the prediction of thermomechanical parameters of the equivalent turning process*

Study of the thermal problem in the chip

Oxley's models applied to equivalent oblique cutting

Oxley has proposed a model which permits to determine the average temperature at the tool/chip interface $\tilde{T}_{int}^{eq}$ [8]. This model is described by the following equation:

$$\tilde{T}_{int}^{eq} = T_{sh}^{eq} + \psi \Delta T_{chip}^{max} \tag{1}$$

Where, ΔT_{chip}^{max} is the maximum temperature rise into the chip, which occurred at the tool-chip interface and $\psi = 0.7$, is a factor that allows for $\tilde{T}_{int}$ being an average value.

The equivalent shearing temperature $\left(T_{sh}^{eq}\right)$ is obtained from the equivalent shearing power $\left(P_{sh}^{eq}\right)$ which is evaluated through the two following expressions.

$$P_{sh}^{eq} = F_{sh}^{eq} V_{sh}^{eq} = \rho c a_p^{eq} t_1^{eq} V_c \left(T_{sh}^{eq} - T_0\right) \tag{2}$$

Where: c is the work material specific heat $(J/Kg°C)$, ρ is the work material density (Kg/m^3), F_{sh}^{eq} is the shearing force and V_{sh}^{eq} is the shearing velocity.

Based on the above equation, T_{sh}^{eq} is given by the following equation:

$$T_{sh}^{eq} = T_0 + \frac{F_{sh}^{eq}}{\rho c a_p^{eq} t_1^{eq}} \frac{\cos \alpha_n^{eq} \cos \lambda_s}{\cos \eta_{sh}^{eq} \cos\left(\phi_n^{eq} - \alpha_n^{eq}\right)} \tag{3}$$

According to Oxley [8], not all the plastic work of chip formation has occurred at the primary shear band. Moreover, according to Boothroyd [16], not all heat generated in the primary shear band is conducted to chip. Thus, the equivalent shearing temperature, based on the above assumptions, is given as follows:

$$T_{sh} = T_0 + \eta(1-\lambda) \frac{F_{sh}^{eq}}{\rho c a_p^{eq} t_1^{eq}} \frac{\cos \alpha_n^{eq} \cos \lambda_s}{\cos \eta_{sh}^{eq} \cos\left(\phi_n^{eq} - \alpha_n^{eq}\right)} \tag{4}$$

Where: $\eta = 0.7$, is the factor that allows the fact that not all the plastic work of chip formation has occurred at the primary shear zone.

The parameter $\lambda\ (0 \leq \lambda \leq 1)$ is the proportion of heat conducted into the workpiece which is determined using the following equation.

$$\begin{cases} \lambda = 0.5 - 0.35\log_{10}\left(R_T \tan\phi_n^{eq}\right) \text{ if } 0.04 \leq R_T \tan\phi_n^{eq} \leq 10 \\ \lambda = 0.3 - 0.15\log_{10}\left(R_T \tan\phi_n^{eq}\right) \text{ if } R_T \tan\phi_n^{eq} > 10 \\ R_T = \frac{\rho c t_1^{eq} V_c}{k} \end{cases} \quad (5)$$

Where, $k(Wm^{-1}K^{-1})$ is the thermal conductivity of workpiece material.

Based on the research work done by Weiner [17], Rapier [18] and Boothroyd [16], Oxley [8] has represented Boothroyd's results by the following equation:

$$\log_{10}\left(\frac{\Delta T_{chip}^{max}}{\Delta \tilde{T}_{chip}}\right) = 0.06 - 0.195\delta\sqrt{\frac{R_T t_2^{eq}}{l_c^{eq}}} + 0.5\log_{10}\left(\frac{R_T t_2^{eq}}{l_c^{eq}}\right) \quad (6)$$

Where: δ is the ratio of the plastic zone thickness to the chip thickness $\left(t_2^{eq}\right)$.

The average temperature rise in the chip ($\Delta\tilde{T}_{chip}$) is determined from the equivalent friction power $\left(P_{int}^{eq}\right)$ generated at the tool-chip interface.

$$P_{int}^{eq} = T_{(t/c)}V_{chip} = \rho c a_p t_1 V_c \Delta\tilde{T}_{chip} \quad (7)$$

Where: V_{chip} is the chip flow velocity and $T_{(t/c)}$ is the tool-chip interfacial force which is determined from the tool-chip interface pressure distribution $\left(p\left(z_{fl}\right)\right)$ and the average friction coefficient $\left(\tilde{f}\right)$. Hence:

$$T_{(c/t)} = \int_0^{l_c} \frac{\tilde{f} a_p p(z_{fl})}{\cos\lambda_s} dz_{fl} = \frac{\tilde{f} a_p l_c p_{max}}{3\cos\lambda_s} \quad (8)$$

Based on the above equations, the average temperature rise in the chip is given as follows:

$$\Delta\tilde{T}_{chip} = \frac{\tilde{f} l_c p_{max} \sin\phi_n}{3\rho c t_1 \cos(\phi_n - \alpha_n)} \quad (9)$$

Numerical approach using Finite Difference Method (FDM)

To predict the position and the maximum value of the tool/chip interface temperature, a numerical simulation is developed based on the Finite Difference Method (FDM). Only the chip is considered and is supposed to have a rectangular form which is defined by its equivalent tool/chip contact length l_c^{eq} and equivalent chip thickness t_2^{eq}. However, effects of equivalent normal shear angle ϕ_n^{eq}, equivalent normal cutting angle α_n^{eq} and equivalent chip flow angle η_c^{eq} are considered in the calculus of the boundary conditions and loadings.

Figure 4 corresponds to the thermal loadings and boundary conditions used to solve the heat equation which governs in the chip. The shearing plane is supposed to be at the same equivalent shearing temperature T_{sh}^{eq}. Surfaces S_1 and S_2 are subject to convection fluxes. The tool/chip interface undergoes a heat flux $Q^{eq}\left(z_{fl}\right)$ which is generated by friction when the chip slides.

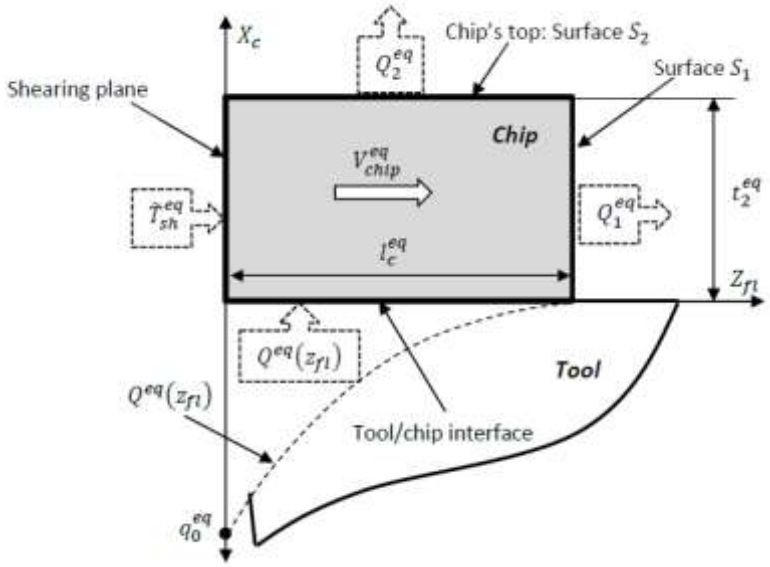

Figure 4. *Thermal loading and boundary conditions*

In the transient state, the general heat equation in the chip is given when two dimensional as follows:

$$\frac{\partial}{\partial z_{fl}}\left(k^{eq}\frac{\partial T}{\partial z_{fl}}\right)+\frac{\partial}{\partial x}\left(k^{eq}\frac{\partial T}{\partial x}\right)-\rho^{eq}c^{eq}V_{chip}^{eq}\left(\frac{\partial T}{\partial z_{fl}}\right)+Q^{eq}(z_{fl})+Q_1^{eq}+Q_2^{eq}= \quad (10)$$

Where: $k^{eq}(mW/mm°C), \rho^{eq}(Ton/mm^3), c^{eq}(mJ/Ton°C)\ and\ t$ are respectively the equivalent thermal conductivity, the equivalent density, the equivalent mass heat capacity of the chip, and the time.

Seven terms were considered in the heat equation which are described as follows:

- $\frac{\partial}{\partial z_{fl}}\left(k\frac{\partial T}{\partial z_{fl}}\right)$: The thermal conduction term according to Z_{fl}
- $\frac{\partial}{\partial x}\left(k\frac{\partial T}{\partial x}\right)$: The thermal conduction term according to X_c
- $\rho^{eq}c^{eq}V_{chip}^{eq}\left(\frac{\partial T}{\partial z_{fl}}\right)$: Advection term
- $Q^{eq}(z_{fl})$: Heat flux generated in the tool/chip interface
- Q_1^{eq}: A convective heat flow which is applied at the surface S_1
- Q_2^{eq}: A convective heat flow which is applied at the surface S_2
- $\rho^{eq}c^{eq}\frac{\partial T}{\partial t}$: Transient term

To solve the heat equation described by the above equation (equation 10), terms $Q^{eq}(z_{fl}), Q_1^{eq}\ and\ Q_2^{eq}$ are determined in the following sections.

Convective heat flows: Q_1^{eq} and Q_2^{eq}

Surfaces S_1 and S_2 of the chip are exposed, respectively, to convective heat flows: Q_1^{eq} and Q_2^{eq}. Q_1^{eq} is applied at surface S_1 and is given by the following equation:

$$Q_1^{eq}=h_1^{eq}(T_1-T_a) \quad (11)$$

Where: h_1^{eq} , T_1 and T_a are, respectively, the equivalent heat convection coefficient, the temperature in surface S_1 and the air temperature.

The convective heat flow Q_2^{eq} is applied at the surface S_2 and is given by the following equation:

$$Q_2^{eq} = h_2^{eq}(T_2 - T_a) \tag{12}$$

Where h_2^{eq} , T_2 and T_a are, respectively, the equivalent heat convection coefficient, the temperature in surface S_2 and the air temperature.

The coefficients of convection h_1^{eq} and h_2^{eq} are expressed in $(mW/(mm^2°C))$ and determined using the dimensionless numbers which are Nusselt's number (Nu), Reynold's number (Re) and Prandtl's number (Pr).

$$\begin{cases} Nu_i^{eq} = \frac{h_i^{eq} d_i^{eq}}{k_a} \\ Re_i^{eq} = \frac{\rho_a V_{chip}^{eq} t_2^{eq}}{\mu_a} \\ Pr_i^{eq} = \frac{\mu_a C_a}{k_a} \end{cases} \tag{13}$$

Where:

- k_a, ρ_a, C_a and μ_a are respectively the thermal conductivity in $(\mathrm{mW/(mm°C)})$, the density in (Ton/mm^3), the mass heat capacity in $\left(mJ/(Ton\,°C)\right)$ and dynamic viscosity in $(Tonne/mms)$ of the air.
- i : is surface index 1 or 2
- d_i^{eq} represents l_c^{eq} for S_2 and t_2^{eq} for S_1

The thermal properties of air are resumed in Table 1.

Table 1. Physical properties of air [19]

Dynamic viscosity $\mu_a(Ton/mms)$	Density $\rho_a(Ton/mm^3)$	Thermal conductivity $K_a(mW/mm°C)$	Mass heat capacity $C_a(mJ/(Ton°C))$
$1{,}850.10^{-11}$	$1{,}177.10^{-12}$	0,0262	1006.10^6

Based on the above equations, the convection coefficient h_i^{eq} are determined using equations as follows:

$$\begin{cases} h_i^{eq} = \frac{2k_a(Re_i)^{0.5}(Pr_i)^{0.33}}{3d_i^{eq}} \; if \; Re_i^{eq} < 3.10^5 \\ h_i^{eq} = \frac{0.036k_a(Re_i)^{0.8}(Pr_i)^{0.33}}{d_i^{eq}} \; if \; Re_i^{eq} > 3.10^5 \end{cases} \tag{14}$$

Heat flux: $Q^{eq}(z_{fl})$

The heat flux $Q^{eq}(z_{fl})$ is supposed to have an exponential evolution with respect to the chip flow direction and resembles to the evolution of tool/chip interface normal pressure $p^{eq}(z_{fl})$ [11].

Thus, the heat flux $Q^{eq}(z_{fl})$ is given as follows:

$$Q^{eq}(z_{fl}) = q_0^{eq}\left(1 - \frac{z_{fl}}{l_c^{eq}}\right)^2 \tag{15}$$

The term q_0^{eq} represents the equivalent maximum heat flux at the tool/chip interface. It is determined from the equivalent thermal power which is evaluated per unit of equivalent length of cut (L_{cut}^{eq}) and generated by friction at the tool/chip interface. Hence, the total thermal power is determined as follows:

$$P_{tot}^{eq} = \frac{T_{(t/c)}^{eq} V_{chip}^{eq}}{L_{cut}^{eq}} \tag{16}$$

Where:

- $T_{(t/c)}^{eq}$ is the equivalent tangential force acted by the tool on the chip in the interface. It is given by the equation as follows:

$$T_{(c/o)}^{eq} = \int_0^{l_c^{eq}} \tilde{f}^{eq} L_{cut}^{eq} p^{eq}(z_{fl}) dz_{fl} = \frac{\tilde{f}^{eq} L_{cut}^{eq} l_c^{eq} p_0^{eq}}{3} \quad (17)$$

- V_{chip}^{i} represents the equivalent chip flow speed and is given as follows:

$$V_{chip}^{eq} = \frac{V_c \sin \phi_n^{eq} \cos \lambda_s}{\cos \eta_c^{eq} \cos(\phi_n^{eq} - \alpha_n)} \quad (18)$$

Based on the above equations, the total thermal power per unit of equivalent length of cut (L_{cut}^{eq}) is given by the following equation:

$$P_{tot}^{eq} = \frac{\tilde{f}^{eq} l_c^{eq} p_0^{eq} V_c \sin \phi_n^{eq} \cos \lambda_s}{3 \cos \eta_c^{eq} \cos(\phi_n^{eq} - \alpha_n)} \quad (19)$$

According to Norouzifard and Hamedi [1], a proportion $\beta = 70\%$ of the equivalent thermal power P_{tot}^{eq} generated at the tool/chip interface is transmitted to the chip. Thus, the total thermal power per unit of equivalent length of cut (L_{cut}^{eq}) transmitted to the chip P_{chip}^{eq} is represented by the following relation:

$$P_{chip}^{eq} = \frac{\beta \tilde{f}^{eq} l_c^{eq} p_0^{eq} V_c \sin \phi_n^{eq} \cos \lambda_s}{3 \cos \eta_c^{eq} \cos(\phi_n^{eq} - \alpha_n)} \quad (20)$$

On the other hand, P_{chip}^{eq} can be determined by the calculus of the integral of the function $Q^{eq}(z_{fl})$ which describes the heat flux distribution along the tool/chip contact. That is way P_{chip}^{eq} is given as follows:

$$P_{chip}^{eq} = \int_0^{l_c^{eq}} Q^{eq}(z_{fl}) dz_{fl} = \frac{q_0^{eq} l_c^{eq}}{3} \quad (21)$$

Based on equations (20 and 21), the term representing the equivalent maximum heat flux at the tool/chip interface is described by the following relation:

$$q_0^{eq} = \frac{\beta \tilde{f}^{eq} p_0^{eq} V_c \sin \phi_n^{eq} \cos \lambda_s}{\cos \eta_c^{eq} \cos(\phi_n^{eq} - \alpha_n)} \quad (22)$$

Boundary conditions

The boundary conditions are as follows:

$$\begin{cases} T(z_{fl} = 0, x) = T_{sh}^{eq} \; pour \; 0 \le x \le t_2^{eq} \\ Q^{eq}(z_{fl}) = -k^{eq} \left.\frac{\partial T}{\partial x}\right|_{x=0} pour \; 0 \le z_{fl} \le l_c^{eq} \\ Q_1^{eq} = h_1^{eq}(T_1 - T_a) = -k^{eq} \left.\frac{\partial T}{\partial z_{fl}}\right|_{z_{fl}=l_c^{eq}} pour \; 0 \le x \le t_2^{eq} \\ Q_2^{eq} = h_2^{eq}(T_2 - T_a) = -k^{eq} \left.\frac{\partial T}{\partial x}\right|_{x=t_2^{eq}} pour \; 0 \le x \le t_2^{eq} \end{cases} \quad (23)$$

Discretization of the heat equation using Finite Difference Method (FDM)

The chip is discretized into elements: $(M-1)$ elements along the equivalent tool/chip contact l_c^{eq} and $(N-1)$ elements along the equivalent chip thickness t_2^{eq}. Thus, it results $(M \times N)$ nodes (Figure 5).

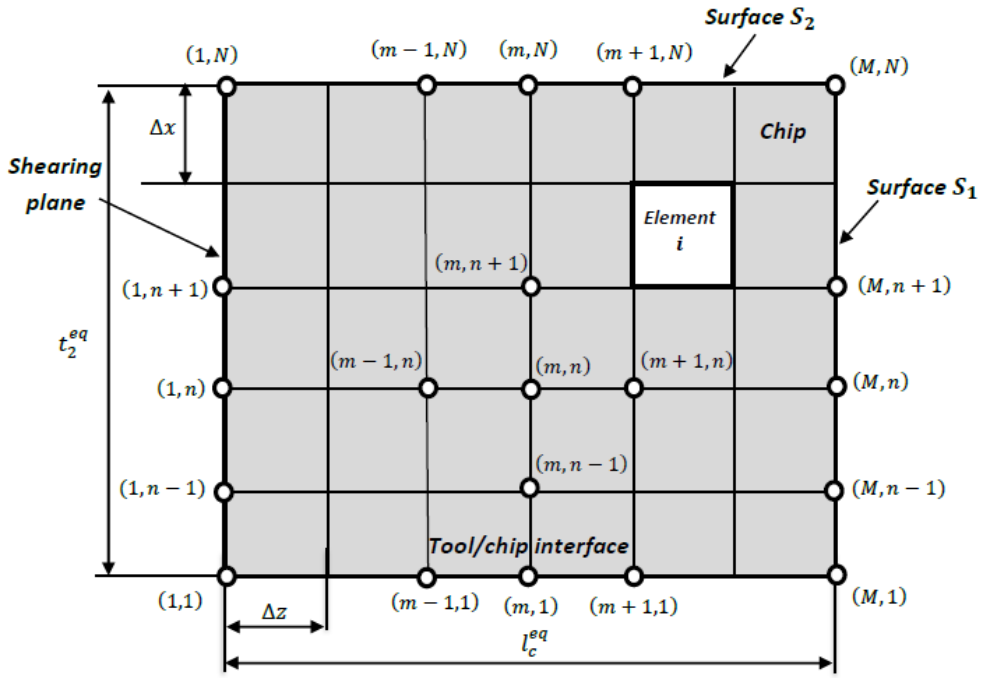

Figure 5. *Chip discretization*

The dimensions of each element are defined as follows:

$$\begin{cases} \Delta z = \frac{l_c^{eq}}{M-1} \\ \Delta x = \frac{t_2^{eq}}{N-1} \end{cases} \tag{24}$$

The increment time is determined by the following relation:

$$\Delta t = \frac{l_c^{eq}}{(N_t-1)V_{chip}^{eq}} \tag{25}$$

Where, M, N and N_t are chosen under the condition of stability as follows:

$$\begin{cases} \frac{\Delta t}{\alpha^{eq}}\left(\frac{1}{\Delta x^2}+\frac{1}{\Delta z^2}\right) \leq \frac{1}{2} \\ \alpha^{eq} = \frac{k^{eq}}{\rho^{eq} c^{eq}} \end{cases} \tag{26}$$

In the present research work, thermal conductivity k^{eq}, mass heat capacity c^{eq} and density ρ^{eq} of the chip material are estimated at the equivalent shearing plane temperature $\tilde{T}_{sh}^{eq}$.

At j^{th} time, the equations in discrete forms are given by:

$$\begin{cases} \frac{\partial^2 T}{\partial x^2} \approx \frac{T_{m,n+1}^j + T_{m,n-1}^j - 2T_{m,n}^j}{(\Delta x)^2} \\ \frac{\partial^2 T}{\partial z_{fl}^2} \approx \frac{T_{m+1,n}^j + T_{m-1,n}^j - 2T_{m,n}^j}{(\Delta z)^2} \\ \frac{\partial T}{\partial z_{fl}} \approx \frac{T_{m+1,n}^j - T_{m-1,n}^j}{2\Delta z} \\ \frac{\partial T}{\partial t} \approx \frac{T_{m,n}^{j+1} - T_{m,n}^j}{\Delta t} \end{cases} \tag{27}$$

Based on boundary conditions and loading, equations in discrete forms, heat equation and the principle of equilibrium at nodes (M,N) and $(M,1)$, temperatures in all nodes are determined by equations as follows:

- Nodes inside chip: $2 \leq m \leq M-1$ et $2 \leq n \leq N-1$

$$T_{m,n}^{j+1} = \left(1 - 2\alpha^{eq}\Delta t\left(\frac{1}{\Delta x^2} + \frac{1}{\Delta z^2}\right)\right)T_{m,n}^{j} + \frac{\alpha^{eq}\Delta t}{\Delta x^2}T_{m,n+1}^{j} + \frac{\alpha^{eq}\Delta t}{\Delta x^2}T_{m,n-1}^{j} + \left(\frac{\alpha^{eq}\Delta t}{\Delta z^2} - \frac{\Delta t V_{chip}^{eq}}{2\Delta z}\right)T_{m+1,n}^{j} + \left(\frac{\alpha^{eq}\Delta t}{\Delta z^2} + \frac{\Delta t V_{chip}^{eq}}{2\Delta z}\right)T_{m-1,n}^{j} \quad (28)$$

- Nodes at tool/chip contact: $2 \leq m \leq M-1$

$$T_{m,1}^{j+1} = \left(1 - 2\alpha^{eq}\Delta t\left(\frac{1}{\Delta x^2} + \frac{1}{\Delta z^2}\right)\right)T_{m,1}^{j} + \frac{2\alpha^{eq}\Delta t}{\Delta x^2}T_{m,2}^{j} + \frac{2\alpha^{eq}\Delta t}{k^{eq}\Delta x}Q_{m,1}^{eq} + \left(\frac{\alpha^{eq}\Delta t}{\Delta z^2} - \frac{\Delta t V_{chip}^{eq}}{2\Delta z}\right)T_{m+1,1}^{j} + \left(\frac{\alpha^{eq}\Delta t}{\Delta z^2} + \frac{\Delta t V_{chip}^{eq}}{2\Delta z}\right)T_{m-1,1}^{j} \quad (29)$$

- Nodes at surface S_1: $2 \leq n \leq N-1$

$$T_{M,n}^{j+1} = \left(1 - 2\alpha^{eq}\Delta t\left(\frac{1}{\Delta x^2} + \frac{1}{\Delta z^2}\right) - \frac{2h_1^{eq}\Delta t}{k^{eq}}\left(\frac{\alpha^{eq}}{\Delta z} - \frac{V_{chip}^{eq}}{2}\right)\right)T_{M,n}^{j} + \frac{\alpha^{eq}\Delta t}{\Delta x^2}T_{M,n+1}^{j} + \frac{\alpha^{eq}\Delta t}{\Delta x^2}T_{M,n-1}^{j} + \frac{2\alpha^{eq}\Delta t}{\Delta z^2}T_{M-1,n}^{j} + \frac{2h_1^{eq}T_a\Delta t}{k^{eq}}\left(\frac{\alpha^{eq}}{\Delta z} - \frac{V_{chip}^{eq}}{2}\right) \quad (30)$$

- Nodes at surface S_2: $2 \leq m \leq M-1$

$$T_{m,N}^{j+1} = \left(1 - 2\alpha^{eq}\Delta t\left(\frac{1}{\Delta x^2} + \frac{1}{\Delta z^2}\right) - \frac{2\alpha^{eq}h_2^{eq}\Delta t}{k^{eq}\Delta x}\right)T_{m,N}^{j} + \frac{2\alpha^{eq}\Delta t}{\Delta x^2}T_{m,N-1}^{j} + \left(\frac{\alpha^{eq}\Delta t}{\Delta z^2} - \frac{\Delta t V_{chip}^{eq}}{2\Delta z}\right)T_{m+1,N}^{j} + \left(\frac{\alpha^{eq}\Delta t}{\Delta z^2} + \frac{\Delta t V_{chip}^{eq}}{2\Delta z}\right)T_{m-1,N}^{j} + \frac{2\alpha^{eq}h_2^{eq}\Delta t}{k^{eq}\Delta x}T_a \quad (34)$$

- Nodes at shearing plane: $1 \leq n \leq N$

$$T_{1,n}^{j+1} = T_{sh} \quad (35)$$

- Nodes of continuity (M,N) and $(M,1)$

$$T_{M,N}^{j+1} = \left(1 - \frac{2h_1^{eq}\Delta t}{k^{eq}}\left(\frac{\alpha^{eq}}{\Delta z} - \frac{V_{chip}^{eq}}{2}\right) - 2\alpha^{eq}\Delta t\left(\frac{1}{\Delta x^2} + \frac{1}{\Delta z^2}\right) - \frac{2\alpha^{eq}h_2^{eq}\Delta t}{k^{eq}\Delta x}\right)T_{M,N}^{j} + \frac{2\alpha^{eq}\Delta t}{\Delta z^2}T_{M-1,N}^{j} + \frac{2\alpha^{eq}\Delta t}{\Delta x^2}T_{M,N-1}^{j} + \frac{2h_1^{eq}T_a\Delta t}{k^{eq}}\left(\frac{\alpha^{eq}}{\Delta z} - \frac{V_{chip}^{eq}}{2}\right) + \frac{2\alpha^{eq}h_2^{eq}\Delta t}{k^{eq}\Delta x}T_a \quad (36)$$

$$T_{M,1}^{j+1} = \left(1 - 2\alpha^{eq}\Delta t\left(\frac{1}{\Delta x^2} + \frac{1}{\Delta z^2}\right) - \frac{2h_1^{eq}\Delta t}{k^{eq}}\left(\frac{\alpha^{eq}}{\Delta z} - \frac{V_{chip}^{eq}}{2}\right)\right)T_{M,1}^{j} + \frac{2\alpha^{eq}\Delta t}{\Delta z^2}T_{M-1,1}^{j} + \frac{2\alpha^{eq}\Delta t}{\Delta x^2}T_{M,2}^{j} + \frac{2\alpha^{eq}\Delta t}{k^{eq}\Delta x}Q_{M,1}^{eq} + \frac{2h_1^{eq}T_a\Delta t}{k^{eq}}\left(\frac{\alpha^{eq}}{\Delta z} - \frac{V_{chip}^{eq}}{2}\right) \quad (37)$$

Equations 28 to 37 can be written with matrix writing as follows:

$$\left[T^{j+1}\right] = [A]\left[T^{j}\right] + [B] \quad (38)$$

Solving the above equation permits to determine temperatures in all nodes at every j^{th} increment of time.

Hybrid analytical-numerical algorithm

The analytical algorithm allows to determine all equivalent thermo-mechanical parameters for the turning process such as cutting temperatures, cutting forces and tribology parameters. To determine the position and the value of the maximum tool/chip interface temperature, a hybrid analytical-numerical algorithm is developed with respect to the assumptions presented in the above sections. The equivalent tool/chip interface temperature $\tilde{T}_{int}^{eq}$, the equivalent tool/chip contact length l_c^{eq}, the equivalent chip thickness t_2^{eq}, the equivalent chip flow velocity V_{chip}^{eq} and the maximum of the equivalent of normal pressure p_0^{eq} at tool/chip interface are determined by the analytical algorithm and thus, they represent the inputs of the numerical algorithm. Besides, the equivalent convection coefficients h_1^{eq} and h_2^{eq} are estimated and the spatial and temporal discretization are done. Finally, equation 38 is resolved and isotherms are known for each time increment. Temperatures for nodes along the tool/chip contact permit to determine the position and the value of the maximum temperature. Figure 6 corresponds to the hybrid flowchart used in the present research work.

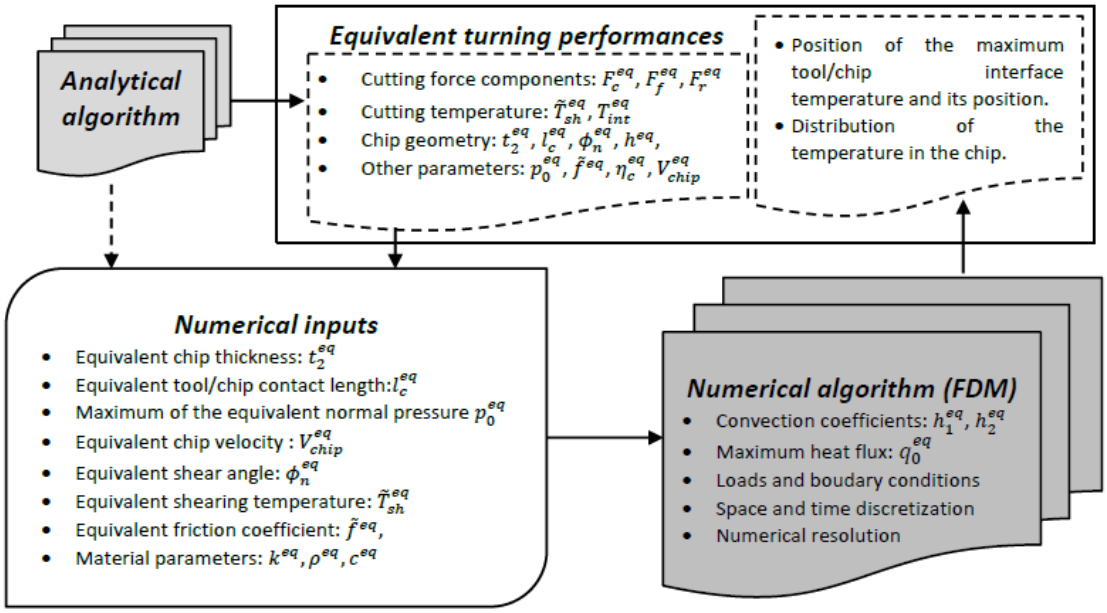

Figure 6. *Hybrid analytical numerical algorithm*

FDM results and discussion

Figures 7 and 8 present results predicted from the numerical simulation by FDM. Oblique cutting with a single cutting edge was considered and four cutting speeds were used (V_c=180, 300, 420 and 540m/min). The workpiece material used in the simulation is AISI304 and its thermal properties and Johnson-Cook parameters are presented in Table 2. Normal cutting angle $\alpha_n = -6°$, inclination angle $\lambda_s = -6°$, edge direction angle $k_r = 75°$, depth of cut $a_p = 1mm$ and uncut chip thickness $t_1 = 0.1mm$.

Table2. Johnson-Cook and thermal parameters of AISI304 [20]

Johnson Cook law: $\tau_{sh} = \frac{1}{\sqrt{3}}\left(A + B\left(\frac{\gamma_{sh}}{\sqrt{3}}\right)^{n}\right)\left\{1 + m\ln\left(\frac{\dot{\gamma}_{sh}}{\dot{\gamma}_0}\right)\right\}\left\{1 - \left(\frac{T_{sh}-T_0}{T_f-T_0}\right)^{\nu}\right\}$						
A	B	n	m	ν	$\dot{\gamma}_0$	T_f (K)
110	1500	0.36	0,014	1	$\frac{1}{\sqrt{3}}$	1694
Thermal properties						
$\boldsymbol{\rho(Kg/m^3)}$	$c(JKg^{-1}K^{-1})$		$k(Wm^{-1}K^{-1})$			
$\mathbf{8193.6 - 0.51T(K)}$	$444.83 + 0.16\mathrm{T(K)}$		$10.86 + 0.014\mathrm{T(K)}$			

Figure 7 corresponds to the temperature distribution in the chip when steady state is reached. It is underlined that the maximum tool/chip interface temperature T_{int}^{max} in the chip increases with respect to cutting speed. However, tool/chip contact length l_c and chip thickness t_2 decrease.

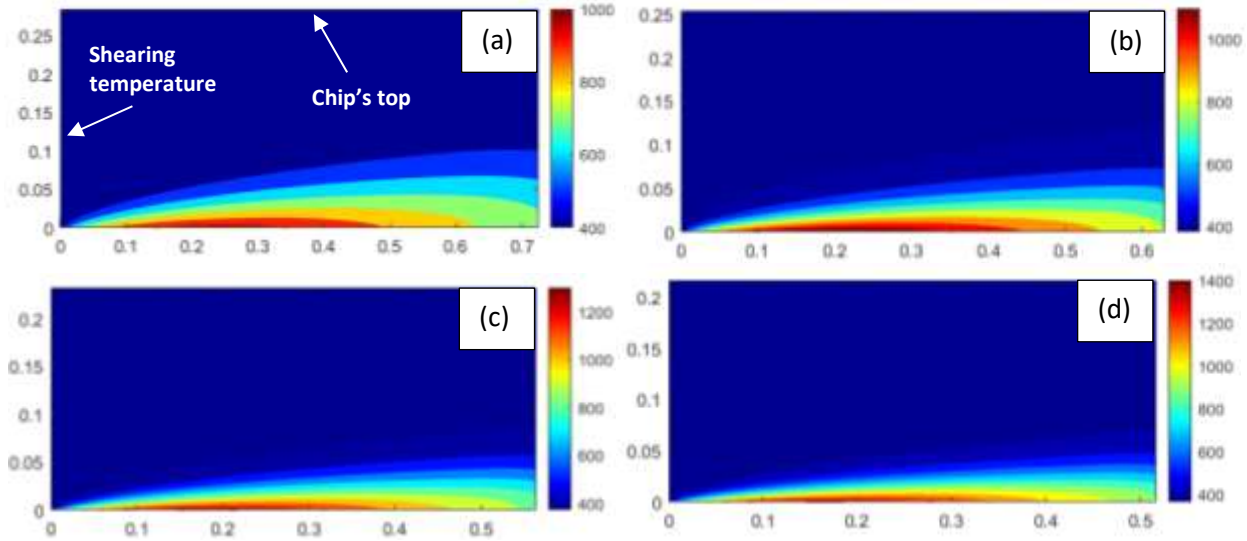

Figure 7. *Isotherm in the chip: Oblique cutting of AISI304: $\alpha_n = -6°$, $\lambda_s = -6°$, $k_r = 75°$, $t_1 = 0.1mm$, $a_p = 1mm$*
(a) $V_c = 180m/min$, (b) $V_c = 300m/min$, (c) $V_c = 420m/min$ and (d) $V_c = 540m/min$

Figure 8 presents the evolution of the tool/chip interface temperature along the tool/chip contact length l_c with respect to z_{fl}. It can be concluded that maximum temperature is situated approximately at $\frac{l_c}{3}$ and approaches the cutting edge as cutting speed increases. Moreover, it is highlighted that the temperature at the chip's top is kept at the shearing temperature T_{sh} and a slight decrease of shearing temperature is noted with respect to cutting speed. Figure 9 corresponds to the evolution of both the position and the maximum tool/chip interface temperature. It is shown that uncut chip thickness significantly affects the position and value of the maximum tool/chip interface temperature. In fact, this temperature increases with uncut chip thickness and its position moves away from the cutting edge.

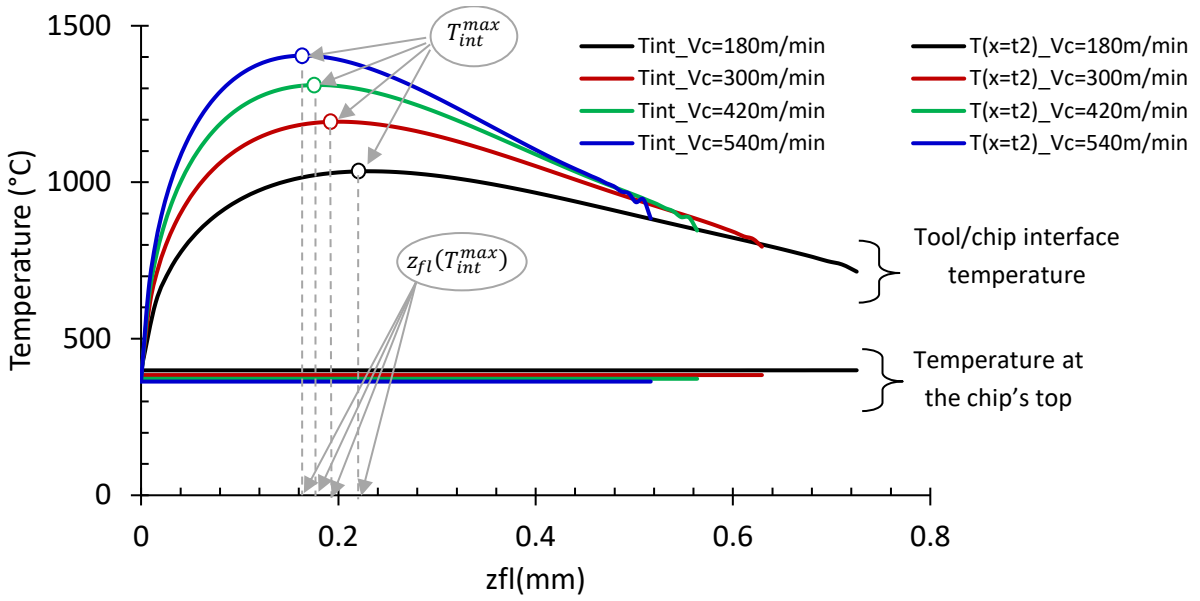

Figure 8. *Evolution of the temperature at the tool/chip interface and chip's top: Oblique cutting of AISI304L:* $\alpha_n = -6°, \lambda_s = -6°, a_p = 1mm; k_r = 75°, t_1 = 0.1mm$

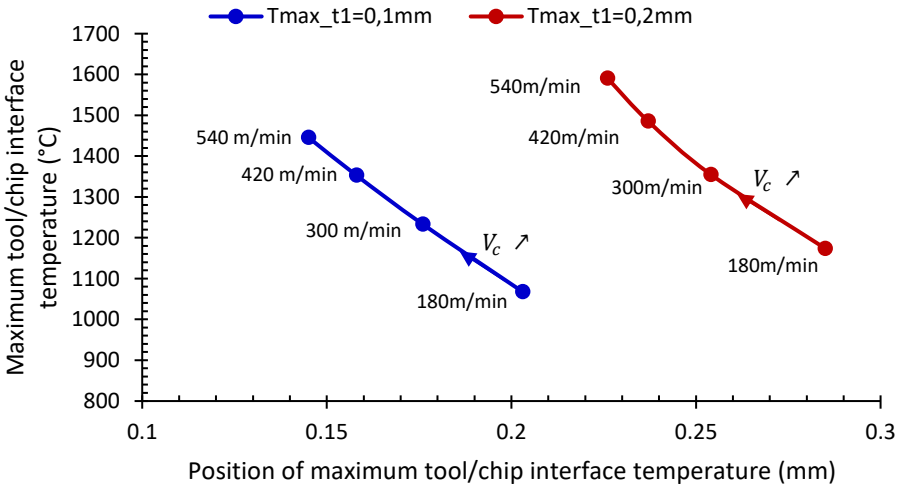

Figure 9. *Evolution of the position and the maximum temperature at the tool/chip interface with respect to cutting speed: Oblique cutting of AISI304L:* $\alpha_n = -6°, \lambda_s = -6°, a_p = 1mm; k_r = 75°$

Figure 10 presents the evolution of the maximum tool/chip interface temperature and its position with respect to time. Two cutting speeds are considered ($V_c = 180\ and\ 420m/min$) and two states were underlined: transient and steady state. The simulation period used represents the sliding time of the chip on the rake face. The transient regime takes about half of this period, then the steady state settles down. Evolution of the position (z_{fl}^{max}) and the maximum value of tool/chip interface temperature (T_{chip}^{max}) with respect to time is drawn in the same curve (Figure 11). It is shown that steady state took place rapidly (about 0.25ms for cutting with $V_c = 180m/min$ and 0.06ms for cutting with $V_c = 420m/min$). Both position and value of T_{chip}^{max} vary when transient regime happened.

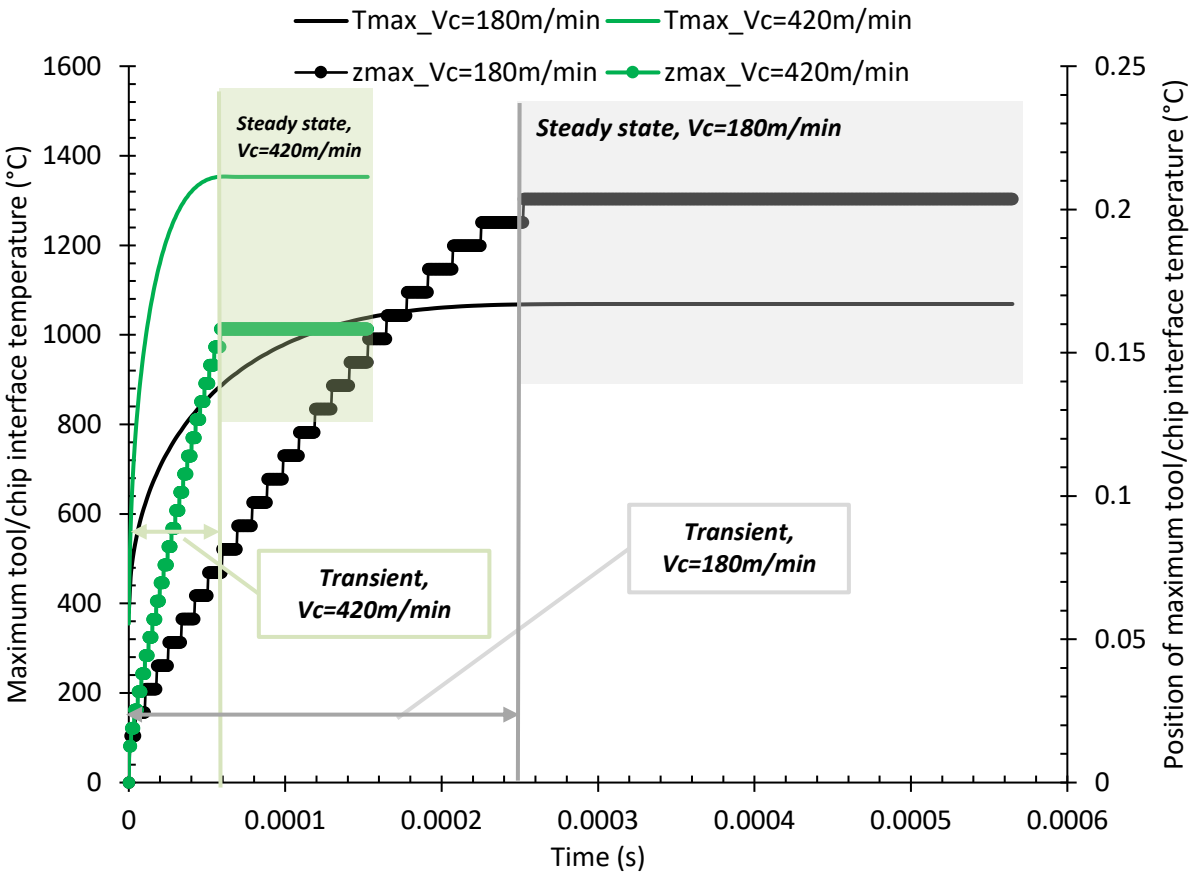

Figure 10. *Evolution of the maximum tool/chip interface temperature and its position with respect to time: Oblique cutting of AISI304: $\alpha_n = -6°$, $\lambda_s = -6°$, $a_p = 1mm$; $k_r = 75°$, $t_1 = 0.1mm$*

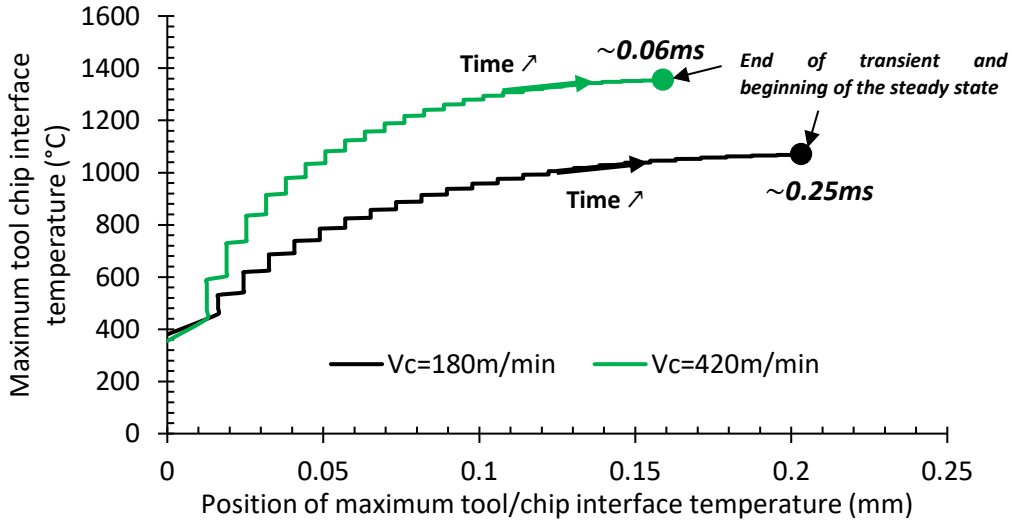

Figure 11. *Evolution of the position and the maximum tool/chip interface temperature with respect to time: Oblique cutting of AISI304: $\alpha_n = -6°$, $\lambda_s = -6°$, $a_p = 1mm$; $k_r = 75°$, $t_1 = 0.1mm$*

Figure 12 corresponds to the evolution of the temperature in the chip when fixing z_{fl} at z_{fl}^{max} and varying x along chip thickness t_2. It is found that the top part of the chip (more than the half) is at the shearing temperature T_{sh}. This remark permits to neglect the convection in the chip's top and consider it at the shearing temperature. Hence boundary condition of the thermal problem can be

changed and the Dirichlet condition (imposed temperature) can be used instead of the Neuman condition (imposed flux).

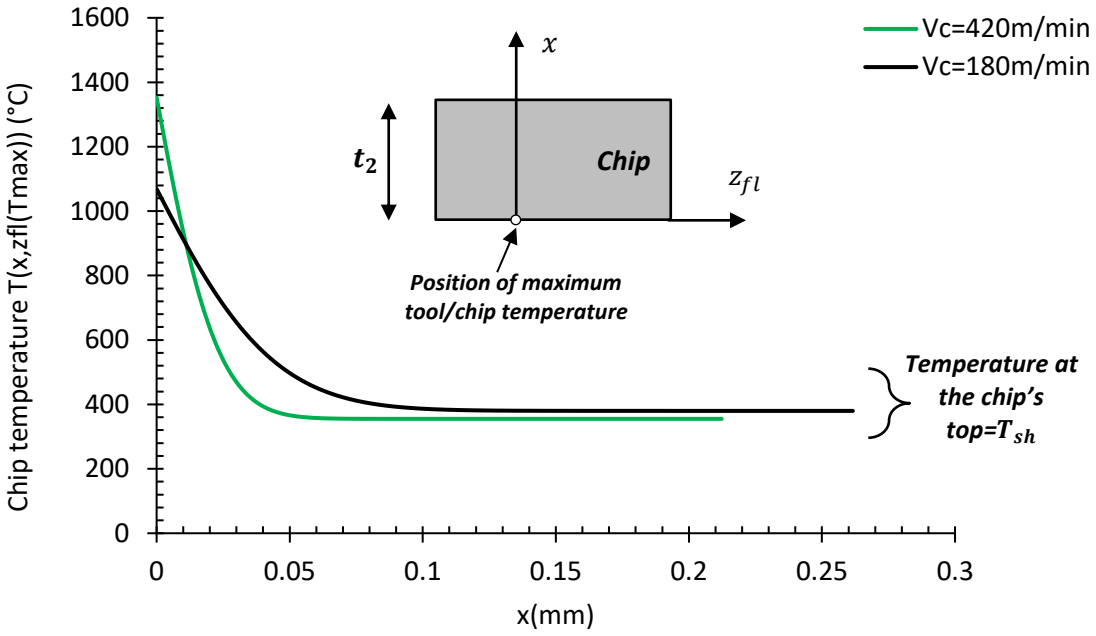

Figure 12. *Evolution of chip temperature along chip thickness at maximum tool/chip temperature position: Oblique cutting of AISI304: $\alpha_n = -6°$, $\lambda_s = -6°$, $a_p = 1mm$; $k_r = 75°$, $t_1 = 0.1mm$*

Analytical approach of thermal problem for equivalent cutting using Laplace transform method

Based on results found in the above section and when neglecting conduction in the direction of motion of the chip (along z_{fl}), thermal problem and boundary conditions can be drawn in Figure 13.

In this section, thermal problem will be solved using Laplace transform method.

Based on the above considerations and adapting steady state, the heat equation in the chip can be described by the following equation:

$$\begin{cases} a\frac{\partial^2 T(z_{fl},x)}{\partial x^2} = V_{chip}^{eq}\frac{\partial T(z_{fl},x)}{\partial z_{fl}}, a = \frac{k^{eq}(\tilde{T}_{sh}^{eq})}{\rho^{eq}(\tilde{T}_{sh}^{eq})c^{eq}(\tilde{T}_{sh}^{eq})} \\ T(z_{fl}=0,x) = \tilde{T}_{sh}^{eq} \\ T(z_{fl},x=t_2^{eq}) = \tilde{T}_{sh}^{eq} \\ -k^{eq}\frac{\partial T(z_{fl},x=0)}{\partial x} = Q^{eq}(z_{fl}) = q_0^{eq}\left(1-\frac{z_{fl}}{l_c^{eq}}\right)^2 \end{cases} \quad (39)$$

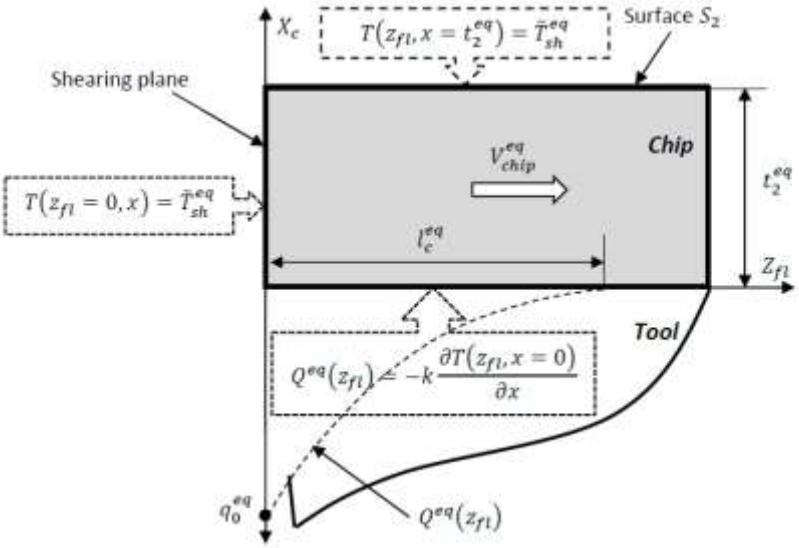

Figure 13. *Thermal loading and boundary conditions*

Through the change of variables $T^*(z_{fl}, x) = T(z_{fl}, x) - \tilde{T}_{sh}^{eq}$, equation 39 becomes

$$\begin{cases} a^{eq}\frac{\partial^2 T^*(z_{fl},x)}{\partial x^2} = V_{chip}^{eq}\frac{\partial T^*(z_{fl},x)}{\partial z_{fl}}, a^{eq} = \frac{k^{eq}(\tilde{T}_{sh}^{eq})}{\rho^{eq}(\tilde{T}_{sh}^{eq})c^{eq}(\tilde{T}_{sh}^{eq})} \\ T^*(z_{fl} = 0, x) = 0 \\ T^*(z_{fl}, x = +\infty) = 0 \\ -k^{eq}\frac{\partial T^*(z_{fl},x=0)}{\partial x} = q_0^{eq}\left(1 - \frac{z_{fl}}{l_c^{eq}}\right)^2 \end{cases} \quad (40)$$

The Laplace transform of $T^*(z_{fl}, x)$ is given as follows:

$$\theta(p, x) = L\left(T^*(z_{fl}, x)\right) = \int_0^{+\infty} T^*(z_{fl}, x)e^{-pz_{fl}}dz_{fl} \quad (41)$$

In the Laplace domain and using Laplace transform properties and theorems, the heat equation becomes as follows:

$$\frac{d^2\theta(p,x)}{dx^2} - \omega^2\theta(p, x) = 0 \quad (42)$$

With $\omega = \sqrt{\frac{p}{a^*}}$ and $a^* = \frac{a^{eq}}{V_{chip}^{eq}}$

Based on the boundary conditions, the solution of the heat equation in the Laplace domain is given as follows:

$$\theta(p, x) = \frac{q_0^{eq}}{k^{eq}}\left(\frac{1}{p\sqrt{\frac{p}{a^*}}}\right)e^{-\omega x} - \frac{2q_0^{eq}}{k^{eq}l_c^{eq}}\left(\frac{1}{p^2\sqrt{\frac{p}{a^*}}}\right)e^{-\omega x} + \frac{2q_0^{eq}}{k^{eq}(l_c^{eq})^2}\left(\frac{1}{p^3\sqrt{\frac{p}{a^*}}}\right)e^{-\omega x} \quad (44)$$

Based on the table of selected Laplace transforms, the equivalent temperature at the tool/chip interface is determined, when considering $x = 0$, and is given by the following equation:

$$T^{eq}(z_{fl}, 0) = \tilde{T}_{sh}^{eq} + \frac{2q_0^{eq}}{\sqrt{\pi k^{eq}(\tilde{T}_{sh}^{eq})\rho(\tilde{T}_{sh}^{eq})c(\tilde{T}_{sh}^{eq})V_{chip}^{eq}}}\left(z_{fl}^{\frac{1}{2}} - \frac{4}{3l_c^{eq}}z_{fl}^{\frac{3}{2}} + \frac{8}{15(l_c^{eq})^2}z_{fl}^{\frac{5}{2}}\right) \quad (45)$$

Where: $q_0^{eq} = \frac{\psi \tilde{f}^{eq} p_0^{eq} V_c \sin \phi_n^{eq} \cos \lambda_s}{\cos \eta_c^{eq} \cos(\phi_n^{eq} - \alpha_n)}$

The average temperature at the tool/chip interface is determined as follows:

$$\tilde{T}_{int}^{eq} = \frac{1}{l_c^{eq}} \int_0^{l_c^{eq}} T^{eq}(z_{fl}, 0) dz_{fl} = \tilde{T}_{sh}^{eq} + \frac{4}{7} q_0^{eq} \sqrt{\frac{l_c^{eq}}{\pi k^{eq}(\tilde{T}_{sh}^{eq}) \rho(\tilde{T}_{sh}^{eq}) c(\tilde{T}_{sh}^{eq}) V_{chip}^{eq}}} \quad (46)$$

The position of the highest temperature at the tool/chip interface is determined from the equation 45 and is given as follows:

$$z_{fl}(T_{int}^{max}) = \frac{(3-\sqrt{3})}{4} l_c^{eq} \approx 0.317 l_c^{eq} \quad (47)$$

The highest temperature at the tool/chip interface is calculated from the following equation:

$$T_{int}^{max} = T^{eq}\left(z_{fl}(T_{int}^{max}), 0\right) = \tilde{T}_{sh}^{eq} + 0.71 q_0^{eq} \sqrt{\frac{l_c^{eq}}{\pi k^{eq}(\tilde{T}_{sh}^{eq}) \rho(\tilde{T}_{sh}^{eq}) c(\tilde{T}_{sh}^{eq}) V_{chip}^{eq}}} \quad (48)$$

Laplace transform results and discussion

Based on the same cutting conditions used in the above section (FDM results and discussion), a comparison between results found with FDM and the analytical approach using Laplace transform (Equation 45) is done (Figure 14). Steady state was considered and very well agreement was found between the two methods. These results are very encouraging and lead to simplifying the thermal problem in metal cutting. Hence, tool/chip interface temperature can be described by equation 45 which also permits to determine the highest one (Equation 48) and its position (Equation 47).

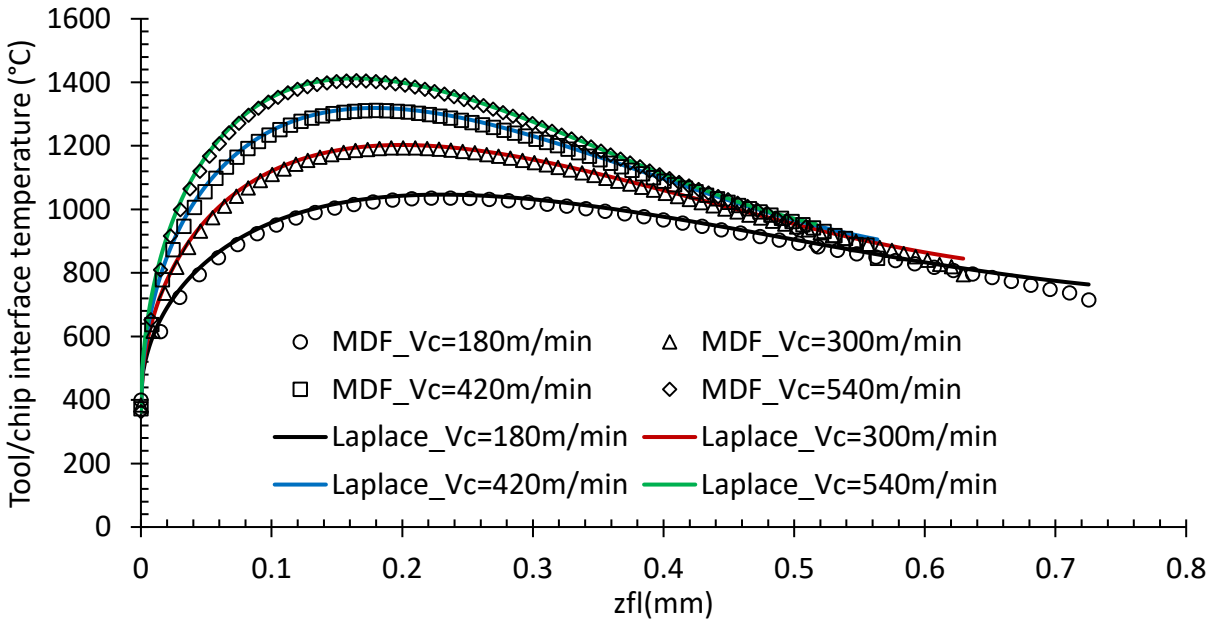

Figure 14. *Comparison between numerical and analytical temperature at the tool/chip interface (Finite difference method and analytical solution with Laplace transforms): Oblique cutting of AISI304L: $\alpha_n = -6°$, $\lambda_s = -6°$, $a_p = 1mm$; $k_r = 75°$, $t_1 = 0.1mm$*

Effects of uncut chip thickness t_1 and cutting speed V_c were studied on the value of maximum tool/chip interface temperature T_{int}^{max} and its position $z_{fl}(T_{int}^{max})$(Figure 15). In fact, T_{int}^{max} increases with cutting speed and uncut chip thickness, however, its position moves away from the cutting edge when t_1 or/and V_c increase.

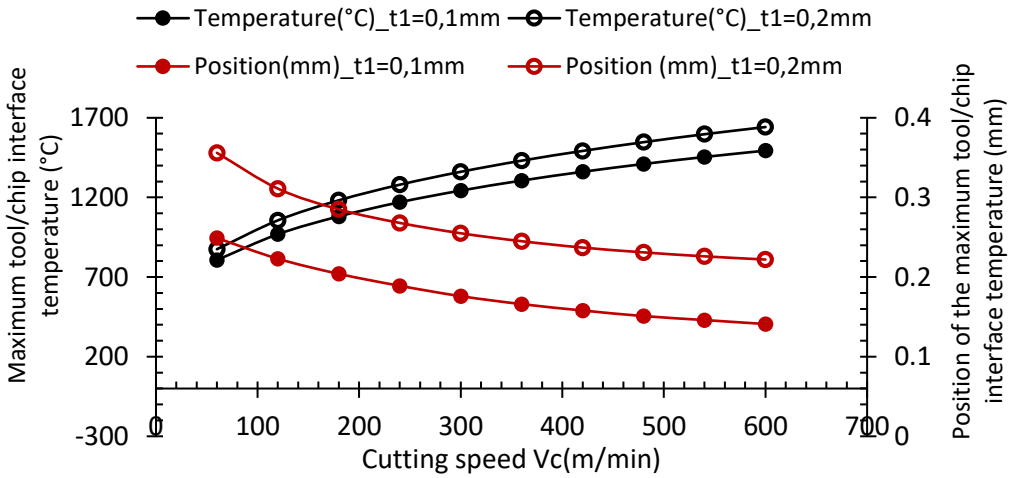

Figure 15. *Evolution of maximum tool/chip interface temperature and its position with respect to cutting speed. Oblique cutting of AISI304L:* $\boldsymbol{\alpha_n = -6°, \lambda_s = -6°, a_p = 1mm; k_r = 75°}$

Average tool/chip interface temperature $\tilde{T}_{int}$ is determined using the approaches presented in this section: Oxley's theory adapted for oblique cutting, Finite Difference Method (FDM) and Analytical approach using Laplace transform. Figure 16 presents a comparison between these three approaches in terms of $\tilde{T}_{int}$. Good agreement is noted between the three approaches and the maximum difference is about 50°C.

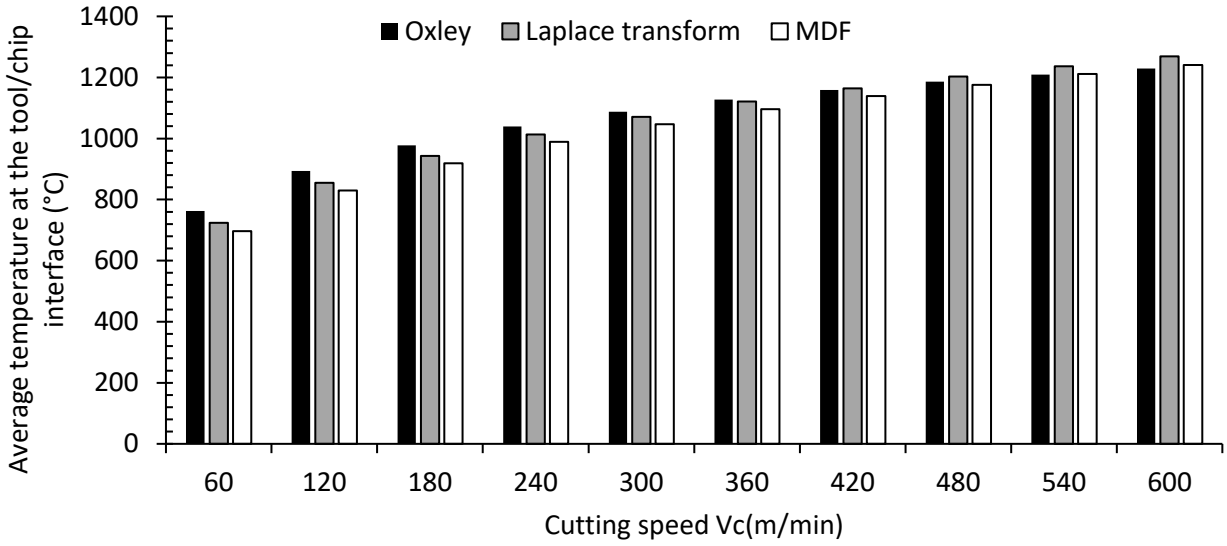

Figure 16. *Comparison between average tool/chip interface temperature (Finite difference method (FDM), analytical solution with Laplace transform (Laplace transform) and modified Oxley's approach): Oblique cutting of AISI304L:* $\boldsymbol{\alpha_n = -6°, \lambda_s = -6°, a_p = 1mm; k_r = 75°, t_1 = 0.1mm}$

Based on the equalities between the expressions of average tool/chip interface temperature $\tilde{T}_{int}$ given by Oxley's theory (Equation 1) and that found with Laplace transform (Equation 46), the partition coefficient β is given by the following equation:

$$\beta \approx 1.225 \frac{\Delta T_{chip}^{max}}{\tilde{f} p_0} \sqrt{\frac{\pi k \rho c}{l_c V_{chip}}} \tag{49}$$

Where ΔT_{chip}^{max} is evaluated by equations (6 and 9) and p_0 is the maximum tool/chip interface pressure.

Figure 14 corresponds to the evolution of partition coefficient β with respect to sliding velocity (V_{chip}). It is shown that β decreases with respect to V_{chip} and it is represented, following a linear regression, by the equation as follows:

$$\beta = 0.765 - 0.026 V_{chip} \tag{50}$$

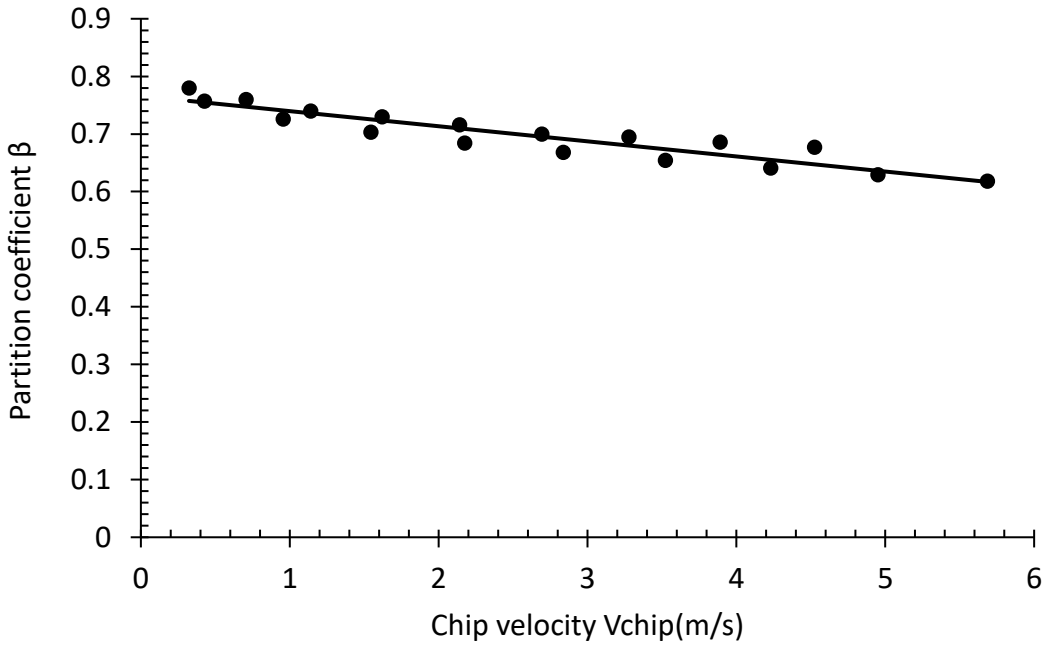

Figure 14. *Evolution of partition coefficient β with respect to chip velocity (sliding speed). Results from simulation of oblique cutting of AISI304*

Experimental results and discussion

For the validation, experimental data for oblique turning with 304 stainless steels conducted by Abdellaoui and Bouzid [11], are used. The tool holder is PCBNL2525M12 (κ_r = 75◦, α_n=−6◦, λ_s=−6◦). The cutting inserts are referenced CNMG120408 and CNMG120412 (r_ε= 0.8mm et r_ε= 1.2mm). According to Sela et al. [21], the cutting-edge radius $r_\beta = 24\ \mu m$. The cutting force components were registered on TRANSMAB 450TD lathe machine using a triaxial force dynamometer KISTLER 9257A. Experimental cutting conditions were conducted using Taguchi array L9, as shown in Table 2.

Table 2. Cutting conditions used in the experiments

Tests	1	2	3	4	5	6	7	8	9
$V_c(m/min)$	180	180	180	250	250	250	400	400	400
$f(mm/rev)$	0.1	0.15	0.2	0.1	0.15	0.2	0.1	0.15	0.2
$a_p(mm)$	0.5	1	2	1	2	0.5	2	0.5	1

When running algorithm1 (Figure 3), results of equivalent parameters were determined and resumed in Table 3. It is noted that the equivalent normal cutting angle has become approximately twice the initial value (α_n=-6°). However, the edge direction angle κ_r decreases and has reached 32° for test 6 when using CNMG120412. Moreover, it decreases with tool nose radius r_ε.

Table 3. Equivalent parameters of oblique turning

Tests	1	2	3	4	5	6	7	8	9
Insert	**CNMG120408: $r_\varepsilon = 0.8mm, r_\beta = 24\mu m$**								
a_p^{eq}(mm)	0.50	1.00	2.00	1.00	2.00	0.50	2.00	0.50	1.00
t_1^{eq}(mm)	0.07	0.13	0.18	0.08	0.14	0.13	0.09	0.10	0.17
α_n^{eq}(°)	-13.37	-12.42	-11.55	-14.25	-12.85	-11.52	-15.15	-13.13	-12.09
κ_r^{eq}(°)	41.98	57.35	65.81	58.14	66.27	39.44	66.71	40.74	56.52
Insert	**CNMG120412: $r_\varepsilon = 1.2mm, r_\beta = 24\mu m$**								
a_p^{eq}(mm)	0.50	1.00	2.00	1.00	2.00	0.50	2.00	0.50	1.00
t_1^{eq}(mm)	0.06	0.11	0.18	0.08	0.13	0.11	0.09	0.08	0.15
α_n^{eq}(°)	-13.08	-12.29	-11.52	-14.08	-12.82	-11.40	-15.11	-13.02	-12.05
κ_r^{eq}(°)	33.88	49.65	62.02	50.31	62.44	31.97	62.84	32.94	48.98

A comparison was made between experimental cutting force components (F_{c_exp}, F_{f_exp} and F_{r_exp}) and those predicted by simulation (F_{c_eq}, F_{f_eq} and F_{r_eq}) using the equivalent model and two inserts were considered: CNMG120408 in Figure 15 and CNMG120412 in Figure 16. Good agreement was be underlined for the two experimental sets. The results found are of great importance because they will allow us to study the equivalent tribological parameters and deduce the equivalent turning performances.

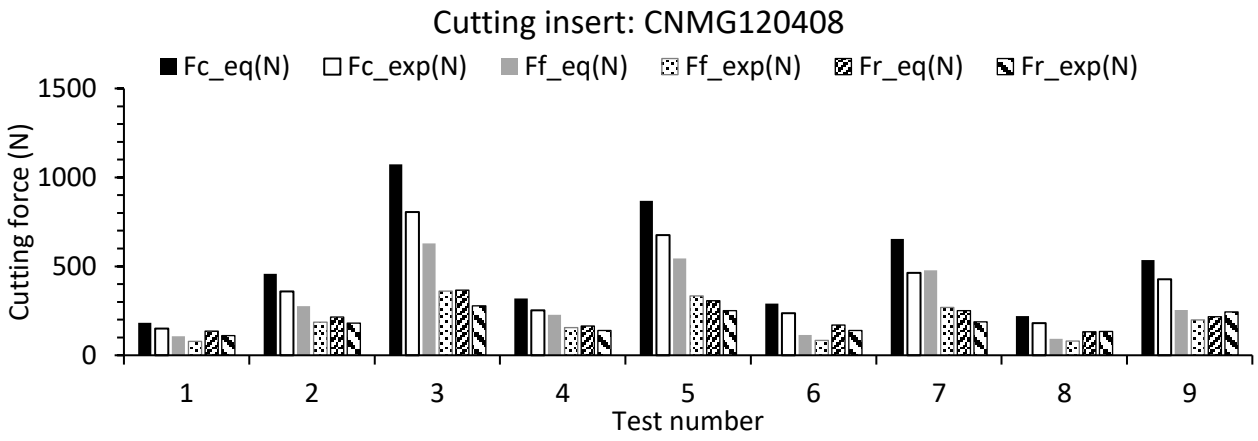

Figure 15. *Comparison between experimental and predicted cutting force components: AISI304L, CNMG120408,* $\alpha_n = -6°, \lambda_s = -6°$

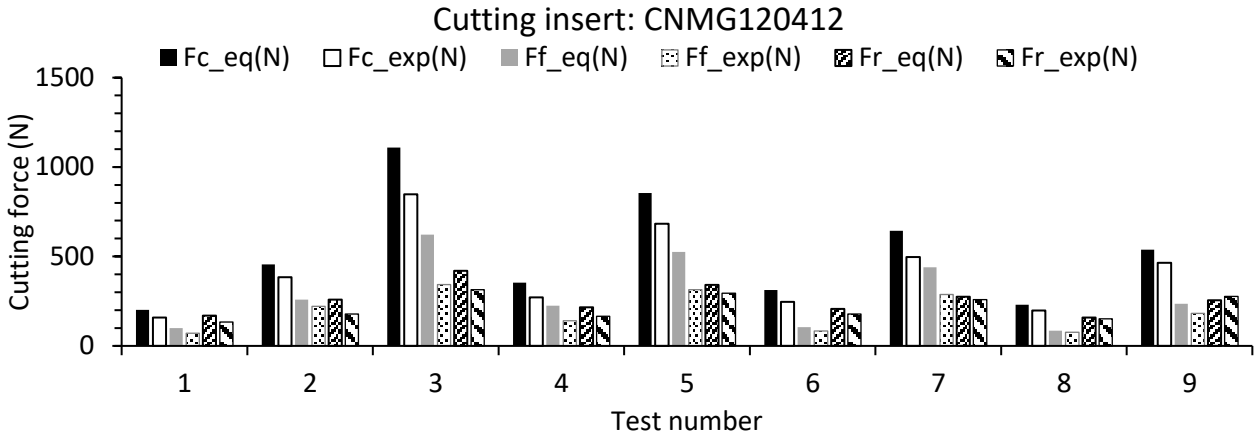

Figure 16. *Comparison between experimental and predicted cutting force components: AISI304L, CNMG120412, $\alpha_n = -6°$, $\lambda_s = -6°$*

Table 4 presents the tribology parameters which are tool/chip contact length, friction coefficient at the tool/chip interface and the maximum too/chip interface temperature and its position. All these parameters were determined, from simulation, for all tests conducted by the two inserts (CNMG120408 and CNMG120412). Besides, a similarity criterion, namely, the Po-criterion $(P_{o\_criterion})$ according to Astakhov [22], is determined. This dimensionless parameter is defined as the ratio of tool/chip contact length l_c to the uncut chip thickness t_1 ($P_{o\_criterion} = \frac{l_c}{t_1}$). According to Astakhov [22] and Abdellaoui and Bouzid [13], cutting performances such as tribology parameters are mainly controlled by this parameter.

When analyzing the results in Table 4, it is underlined that T_{int}^{max} is between 1200°C and 1500°C for all tests. The highest one was determined for test 9 and the lowest one for test 1. This result was confirmed with two inserts. Moreover, it can be highlighted that T_{int}^{max} decreases with tool nose radius r_ε and this result was confirmed by the work of Abdellaoui et al. [14] and Kishawy [12]. This decrease seems to be due to the increase of the tool-workpiece contact surface which promotes the thermal exchange. However, the equivalent oblique cutting considered in the present research work agrees well with this result.

Table 4. **Equivalent tribology parameters**

Tests	**1**	**2**	**3**	**4**	**5**	**6**	**7**	**8**	**9**
Insert	**CNMG120408: $r_\varepsilon = 0.8mm, r_\beta = 24\mu m$**								
$T_{int\_max}^{eq}$(°C)	1227	1266	1281	1329	1365	1347	1429	1468	1508
$z_{fl}(T_{int\_max}^{eq})$(mm)	0.13	0.20	0.25	0.14	0.20	0.19	0.17	0.15	0.23
l_c^{eq}(mm)	0.42	0.63	0.78	0.45	0.64	0.59	0.53	0.46	0.72
$\tilde{f}^{eq}$	0.58	0.46	0.41	0.51	0.42	0.44	0.45	0.43	0.36
Po_criterion	6.00	4.85	4.33	5.62	4.57	4.53	5.88	4.60	4.23
Insert	**CNMG120412: $r_\varepsilon = 1.2mm, r_\beta = 24\mu m$**								
$T_{int\_max}^{eq}$(°C)	1208	1246	1280	1325	1357	1321	1459	1437	1486

$z_{fl}(T_{int\ max}^{eq})$(mm)	0.12	0.18	0.25	0.15	0.19	0.17	0.15	0.13	0.21
l_c^{eq}(mm)	0.39	0.58	0.78	0.46	0.61	0.55	0.47	0.41	0.66
$\tilde{f}^{eq}$	0.61	0.50	0.41	0.51	0.43	0.47	0.44	0.47	0.38
Po_criterion	6.50	5.27	4.33	5.75	4.69	5	5.22	5.12	4.40

The evolutions of maximum tool/chip interface temperature T_{int}^{max} and average tool/chip friction coefficient $\tilde{f}$ are given in Figure 17. It is revealed that T_{int}^{max} decreases with the dimensionless number P_o, however, the friction coefficient increases. This result seems to be correct because T_{int}^{max} increases with cutting speed however tool/chip contact length l_c decreases and so necessary the dimensionless number P_o. On the other hand, and according to Abdellaoui and Bouzid [13] and Mustapha et al. [23], average friction coefficient $\tilde{f}$ decreases with average tool/chip interface temperature $\tilde{T}_{int}$ and uncut chip thickness t_1. Moreover, when t_1 increases slightly, l_c increases significantly and consequently the dimensionless number P_o, too. Therefore, the average tool/chip interface temperature decreases and induces an increase in the average friction coefficient.

Following a linear regression, the maximum tool/chip interface temperature V_{chip} and the friction coefficient $\tilde{f}$ are given by the following equations:

$$T_{int}^{max} = 1667.6 - 63.15P_o \tag{51}$$

$$f = 0.08 + 0.07P_o \tag{52}$$

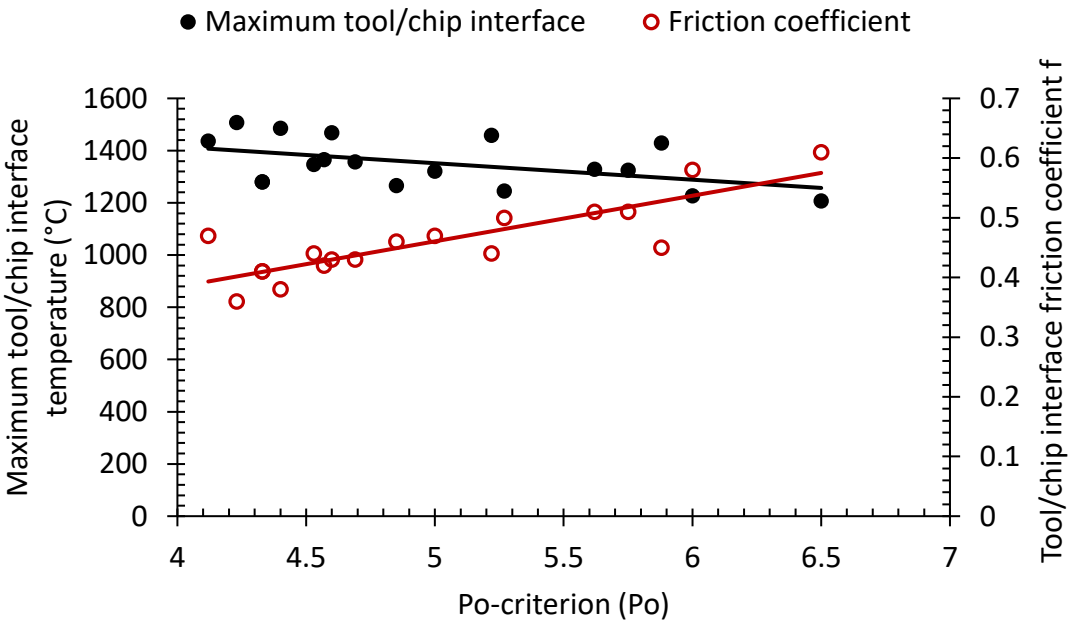

Figure 17. *Evolution of maximum tool/chip interface temperature and tool/chip interface coefficient with respect to Po-criterion (Po)*

Conclusion

In the present paper, turning performances were determined using equivalent oblique cutting with a single cutting edge. Equivalent tool parameters and equivalent cutting conditions were evaluated considering the effects of tool nose and edge radii. The results are used in a thermomechanical

algorithm which is controlled by one loop with respect to average tool/chip interface temperature. All equivalent thermomechanical parameters such as cutting force components, cutting temperatures and tribology parameters were determined with a good accuracy.

To determine the maximum tool/chip interface temperature and its position, a hybrid analytical-numerical algorithm was used. The thermal problem in the chip is resolved in the first time using the Finite Difference Method (FDM) considering transient regime. It is concluded that a steady state takes place rapidly and a transient regime can be omitted in the resolution of the heat equation in the chip. Besides, the chip's top was considered as a convection surface, however numerical results show that it can be considered as a Dirichlet condition (fixed temperature) instead of a Neumann one (heat flux across the boundaries).

Based on the considerations drawn from numerical results, steady state and a fixed temperature in the chip's top were considered. The thermal problem was resolved again using Laplace transforms. The evolution of tool/chip interface temperature was represented by an equation that permits to determine the highest temperature and its position at the tool/chip interface. Good agreement was underlined between numerical (FDM) and analytical (Laplace transform) results which proves the simplification used in the heat equation. Moreover, it was determined that the maximum tool/chip interface temperature is situated far from the cutting edge about $0.317 l_c$.

The average tool/chip interface temperature was evaluated using three approaches (FDM, Laplace transform and Oxley's theory) and good agreement was noted. Using this equality, the partition coefficient was represented by an equation with respect to the sliding velocity of the chip. It was found that the partition coefficient is strongly related to sliding speed. However, it decreases about 20% when chip velocity increases from 1 to 5m/s.

Experimental data for oblique cutting with 304 stainless steels were used and all equivalent parameters were evaluated. Good agreement was noted in terms of cutting force components, between experiments and predicted results using the equivalent oblique cutting model. Tribology parameters at the tool/chip interface as like maximum tool/chip interface temperature T_{int}^{max} and its position, tool/chip contact length l_c and average friction coefficient $\tilde{f}$ were evaluated for all tests. It was concluded that T_{int}^{max} and $\tilde{f}$ were mainly controlled by the Po-criterion (P_o). In fact, T_{int}^{max} decreases with P_o however $\tilde{f}$ increases.

As a perspective, the equivalent oblique cutting model will be used to predict all turning performances over a wide range of cutting conditions. Crater wear and tool life will be studied with respect to tribological parameters for each couple workpiece-tool (CWT).

Nomenclature

a_p	Cutting depth [mm]
a_p^{eq}	Equivalent depth of cut [mm]
c^{eq}	Equivalent work material specific heat [$JKg^{-1}K^{-1}$]
f	Feed rate [mm/rev]
$\tilde{f}$	Average coefficient of friction at tool-chip interface
$\tilde{f}^{eq}$	Equivalent average coefficient of friction at tool chip interface
F_c^{eq}	Equivalent tangential force [N]
F_f^{eq}	Equivalent feed force [N]
F_r^{eq}	Equivalent radial force [N]
F_{sh}^{eq}	Equivalent shearing force [N]
k^{eq}	Equivalent work material thermal conductivity [$Wm^{-1}K^{-1}$]
l_c^i	Tool-chip contact length for element *i* [mm]
p_0^{eq}	equivalent of maximum normal stress at tool-chip contact [N/mm^2]
r_β	Cutting edge radius [mm]
r_ε	Tool-nose radius [mm]
t_1	Uncut chip thickness [mm]
t_2^{eq}	equivalent chip thickness [mm]
T_f	Workpiece melting temperature [K]
T_0	Initial work-piece temperature [K]
T_{sh}^{eq}	Equivalent shearing temperature [K]
$\tilde{T}_{int}^{eq}$	Average tool-chip interface temperature [K]
V_c	Cutting speed [m/min]
V_{chip}^{eq}	Equivalent chip velocity [mm/s]
V_{sh}^{eq}	Equivalent shearing velocity [mm/s]
α_n	Normal rake angle [°]
δ	Secondary shear zone thickness ratio to chip thickness
ϕ_n^{eq}	Equivalent normal shear angle [°]
γ_{sh}^{eq}	equivalent shear strain
$\dot{\gamma}_{sh}^{eq}$	Equivalent shear strain rate
η_c^{eq}	Equivalent chip flow angle [°]
η_{sh}^{eq}	Shearing direction angle [°]
κ_r	Edge direction angle [°]
κ_r^{eq}	Equivalent edge direction angle [°]

λ_s Edge inclination angle [°]

ρ^{eq} Equivalent work material density [Kg/m^3]

τ_{sh}^{eq} Equivalent shear stress [N/mm²]

Funding

This work is carried out with the support and funding allocated to the Unit of Mechanical and Materials Production Engineering (UGPMM/UR17ES43) by the Tunisian Ministry of Higher Education and Scientific Research.

Declarations

Competing interests: The authors declare that there is no conflict of interest.

Availability of data and materials: All data and materials used to produce the results in this article can be obtained upon request from the corresponding authors.

Availability of code: Code used to produce the results in this article can be obtained upon request from the corresponding authors

Ethics approval: The authors declare that there is no ethical issue applied to this article.

Consent to participate: The authors declare that all authors have read and approved to submit this manuscript to IJAMT.

Consent to publish: The authors declare that all authors agree to sign the transfer of copyright for the publisher to publish this article upon on acceptance.

Contributions: All the above-mentioned authors contributed to the manuscript equally.

References

[1] **Norouzifard, V., Hamedi, (2014)** M. A three-dimensional heat conduction inverse procedure to investigate tool–chip thermal interaction in machining process. Int J Adv Manuf Technol 74, 1637–1648 (2014). https://doi.org/10.1007/s00170-014-6119-6

[2] **Hao, G., Liu, Z. (2020)** The heat partition into cutting tool at tool-chip contact interface during cutting process: a review. Int J Adv Manuf Technol 108, 393–411 (2020). https://doi.org/10.1007/s00170-020-05404-9

[3] **Puls H, Klocke F, Veselovac D (2016)** FEM-based prediction of heat partition in dry metal cutting of AISI 1045. Int J Adv Manuf Technol 86(1-4):737–745

[4] **Huang, S., Tao, B., Li, J. et al. (2018)** On-line estimation of the tool-chip interface temperature field during turning using a sequential inverse method. Int J Adv Manuf Technol 97, 939–952 (2018). https://doi.org/10.1007/s00170-018-1987-9

[5] **Kus, Abdil, Yahya Isik, M. C. Cakir, Salih Coşkun, and Kadir Özdemir. 2015.** "Thermocouple and Infrared Sensor-Based Measurement of Temperature Distribution in Metal Cutting" *Sensors* 15, no. 1: 1274-1291. https://doi.org/10.3390/s150101274

[6] **Merchant M.E. (1945),** Mechanics of the metal cutting process: I-Orthogonal cutting and a type 2 chip, J. Applied physics 16, n.5, 1945, P. 267**.**

[7] **Lee E. H., Shaffer B. W. (1951),** The theory of plasticity applied to the problem of machining. ASME, Journal of Applied Mechanics 18. 405-413. 1951.

[8] **Oxley P. L. B. (1998)** DEVELOPMENT AND APPLICATION OF A PREDICTIVE MACHINING THEORY, Machining Science and Technology, 2:2, 165-189, DOI: 10.1080/10940349808945667

[9] **Moufki A., Devillez A., Dudzinski D., Molinari A. (2004),** Thermomechanical modelling of oblique cutting and experimental validation, International Journal of Machine Tools & Manufacture 44 (2004) 971-989

[10] **Li, B.; Hu, Y.; Wang, X.; Li, C.; Li, X. (2011)** An analytical model of oblique cutting with application to end milling. Machining Science and Technology: An International Journal, 15(4): 453–484.

[11] **Abdellaoui Lefi & Bouzid Wassila (2016)** Thermomechanical approach for the modeling of oblique machining with a single cutting edge, Machining Science and Technology, 20:4, 655-680, DOI: 10.1080/10910344.2016.1224020

[12] **Kishawy H. A. (2002)** An experimental evaluation of cutting temperatures during high-speed machining of hardened D2 tool steel, Machining science and technology, vol. 6(1), pp. 67-79.

[13] **Abdellaoui Lefi & Bouzid Wassila (2016)** Thermomechanical modeling of oblique turning in relation to tool-nose radius, Machining Science and Technology, 20:4, 586-614, DOI: 10.1080/10910344.2016.1224017

[14] **Abdellaoui Lefi, Khlifi Hassen, Wassila Bouzid Sai & Hedi Hamdi (2021)** Tool nose radius effects in turning process, Machining Science and Technology, 25:1, 1-30, DOI: 10.1080/10910344.2020.1815038

[15] **Khlifi, H., Abdellaoui, L. & Bouzid Sai, (2019)** An equivalent geometry model for turning tool with nose and edge radii W. Int J Adv Manuf Technol (2019) 103 : 4233. https://doi.org/10.1007/s00170-019-03787-y

[16] **Boothroyd, G. (1963)** Temperature in orthogonal metal cutting. Proceedings of the Instrumentation and Mechanical Engineering, 177(29): 789.

[17] **Weiner, J.H. (1955)** Shear plane temperature distribution in orthogonal cutting. Transactions of the American Society Mechanical Engineers, 77: 1331.

[18] **Rapier, A.C. (1954)** A theoretical investigation of the temperature distribution in the metal cutting process. British Journal of Applied Physics, 5: 400.

[19] **Bouzid, W. (1993)** Etude expérimentale et numérique de la coupe orthogonale. PhD Thesis, ENSAM.

[20] **Lurdos, O. (2008)** Lois de comportement et de recristallisation dynamique: Approche empiriques et physique, Thèse, Ecole Nationale Supérieur des Mines, Saint-Etienne.

[21] **Sela A., Ortiz-de-Zarate G., Arrieta I., Soriano D., Aristimuño P., Medina-Clavijo B. and Arrazola P.J. (2019).** A mechanistic model to predict cutting force on orthogonal machining of Aluminum 7475-T7351 considering the edge radius. 17th CIRP Conference on Modelling of Machining Operations (17th CIRP CMMO). https://doi.org/10.1016/j.procir.2019.04.066.

[22] **Astakhov, V.P. (2006)** Tribology of Metal Cutting, Tribology and Interface Engineering Series, No 52; Briscoe, B.J.; Eds, London: Elsevier.

[23] **Mustapha A., Fritz K., Dieter L., Dražen V. (2015)** The mechanics of cutting: In-situ measurement and modelling, 15th CIRP Conference on Modeling of Machining Operations, Procedia CIRP, vol. 31, pp. 246–251.